Computational Studies of the Kinetics of the C + NO and O + CN Reactions

Stefan Andersson,[†] Nikola Marković,[‡] and Gunnar Nyman*[,†]

Department of Chemistry, Physical Chemistry, Göteborg University, SE-412 96 Göteborg, Sweden, and Department of Chemistry and Bioscience, Chalmers University of Technology, SE-412 96 Göteborg, Sweden

Received: October 21, 2002; In Final Form: April 30, 2003

Thermal rate coefficients for the reactions $C(^3P) + NO(X^2\Pi) \rightarrow CN(X^2\Sigma^+) + O(^3P)$, $C(^3P) + NO(X^2\Pi) \rightarrow CO(X^1\Sigma^+) + N(^2D)$, and $O(^3P) + CN(X^2\Sigma^+) \rightarrow CO(X^1\Sigma^+) + N(^2D)$ in the temperature range from 5 to 5000 K have been obtained using quasiclassical trajectory calculations. Results are reported for two ab initio potential energy surfaces corresponding to states of $^2A'$ and $^2A''$ symmetry. Good agreement between calculated and experimental rate coefficients are obtained for the C + NO reactions for all temperatures, whereas the rate coefficient for the O + CN reaction at room temperature is larger than that found experimentally. The dynamics is considerably different on the two potential energy surfaces with the $^2A''$ giving rate coefficients in better agreement with experiments. The quality of the potential energy surfaces are discussed in the light of new electronic structure calculations including spin−orbit coupling.

1. Introduction

The reactive systems $C(^3P) + NO(X^2\Pi)$ and $O(^3P) + CN(X^2\Sigma^+)$ have received attention from molecular astrophysicists[1−5] and combustion scientists,[6−14] alike. Three of the possible reactions are exothermic

$$C(^3P) + NO(X^2\Pi) \rightarrow CN(X^2\Sigma^+) + O(^3P) \quad (1)$$

$$C(^3P) + NO(X^2\Pi) \rightarrow CO(X^1\Sigma^+) + N(^2D) \quad (2)$$

and

$$O(^3P) + CN(X^2\Sigma^+) \rightarrow CO(X^1\Sigma^+) + N(^2D) \quad (3)$$

The C + NO reaction has been of interest as part of the process of nitrogen reburning, i.e., the removal of NO and eventual formation of N_2, in high-temperature combustion. The O + CN reaction has also received attention as a possible major source of depletion of CN both in combustion[13] and in dense interstellar clouds.[1,3] For the latter application, it is believed that this reaction could be the most important source of CN destruction. Because CN is a possible precursor to complex molecules, such as cyanopolyynes, the detailed knowledge of the rate of the O + CN reaction could be crucial to the understanding of the chemical evolution of interstellar clouds. There have been a number of measurements of the rate coefficients for these reactions. These are summarized in Tables 1−3. It is seen that there are large deviations between the experiments at room temperature for both the C + NO and O + CN systems. No measurements of low-temperature rate coefficients for the latter reaction have been reported. Previous theoretical work has been discussed in ref 15.

In this paper, we present quasiclassical trajectory calculations using two potential energy surfaces corresponding to electronic states of $^2A'$ and $^2A''$ symmetry. From these calculations, we have obtained thermal rate coefficients that are compared to experimental data. In section 2, we give the details about the calculations, and in section 3, the obtained results are presented and discussed. Finally, a few concluding remarks are given in section 4.

TABLE 1: Thermal Rate Coefficients for the C + NO Reaction

	year	*T*/K	$k/10^{-11}$ cm^3 molecule^{-1} s^{-1}
Chastaing et al.[32]	2000	15	22.8 ± 1.7
Chastaing et al.[32]	2000	27	20.1 ± 1.1
Chastaing et al.[32]	2000	54	25.0 ± 0.8
Chastaing et al.[32]	2000	83	17.3 ± 2.6
Chastaing et al.[32]	2000	207	16.9 ± 1.5
Chastaing et al.[32]	2000	295	12.0 ± 0.1
Lindackers et al.[43]	1990	2720−3810	3.3 ± 0.7
Dean et al.[34]	1991	1550−4050	8.0 ± 3.6

TABLE 2: Room Temperature Rate Coefficients for the C + NO Reaction

	year	$k/10^{-11}$ cm^3 molecule^{-1} s^{-1}
Braun et al.[44]	1969	11
Husain and Kirsch[45]	1971	7.3 ± 2.2
Husain and Young[46]	1974	4.8 ± 0.8
Becker et al.[47]	1988	1.6 ± 0.2
Dorthe et al.[48]	1991	2.7 ± 0.3
Bergeat et al.[33]	1999	5.4 ± 0.8
Chastaing et al.[32]	2000	12.0 ± 0.1

2. Computational Details

2.1. Potential Energy Surfaces. Our dynamics calculations are performed on two different potential energy surfaces (PES). These surfaces correspond to electronic states of $^2A'$ and $^2A''$ symmetry and constitute a Born−Oppenheimer basis for the true Renner−Teller coupled ground state of the CNO system.[16] For linear configurations the surfaces are degenerate and correspond to an electronic state of $^2\Pi$ symmetry. The analytic forms of the surfaces are of a many-body expansion (MBE) type, and they have been produced by fitting these expressions to approximately 2400 energy points, out of which about 1000 are ab initio (CASPT2) points and the rest are calculated from

* To whom correspondence should be addressed. Fax: +46 31 167194. E-mail: nyman@phc.gu.se.
[†] Göteborg University.
[‡] Chalmers University of Technology.

10.1021/jp0222604 CCC: $25.00
Published on Web 06/20/2003

TABLE 3: Thermal Rate Coefficients for the O + CN Reaction

	year	T/K	$k/10^{-11}$ cm^3 molecule^{-1} s^{-1}
Schmatjko and Wolfrum[35]	1978	298	1.7 ± 0.7
Titarchuk and Halpern[36]	1995	298	3.69 ± 0.75
Boden and Thrush[49]	1968	570−687	$(10.5 \pm 5.8) \exp[(-1200 \pm 350)/T]$
Louge and Hanson[38]	1984	2000	$3.0 + 2.6/-1.3$
Davidson et al.[37]	1991	3000−4500	13.0 ± 2.6

TABLE 4: Arrangement Channels: Comparison between Our PESs and Experimental Data (Italic)[a]

	$\Delta\epsilon_0$	r_e	ω_e
C + NO	0	1.161	1883
	0	*1.151*	*1904*
O + CN	−1.22	1.187	1998
	−1.26	*1.172*	*2069*
N(^{2}D) + CO	−2.03	1.140	2141
	−2.21	*1.128*	*2170*
N(^{4}S) + CO[b]	−4.51	1.140	2141
	−4.59	*1.128*	*2170*

[a] Experimental diatomic data are taken from ref 27 and atomic data from ref 50. Exothermicities are relative to C + NO and are quoted in eV, equilibrium distances are in Å, and harmonic frequencies are in cm^{-1}. [b] This channel is not included in our PESs. The data presented is derived from our diatomic potentials.

TABLE 5: Most Important Stationary Points on the Analytic PESs[a]

	R_{CN}	R_{NO}	R_{CO}	V	ω_1	ω_2	ω_3	ω_4
Linear Minima								
CNO	1.226	1.221	2.447	−4.213	1851	1087	532	532
	1.227	*1.220*	*2.446*	*−4.214*	*1838*	*1164*	*287*	*287*
NCO	1.241	2.423	1.182	−6.901	1859	1189	680	680
	1.239	*2.427*	*1.188*	*−6.906*	*1877*	*1265*	*518*	*518*
CON	2.514	1.303	1.211	−1.734	1482	922	476	476
	2.521	*1.308*	*1.213*	*−1.735*	*1455*	*932*	*366*	*366*
Triangular Minimum ($^2A''$)								
Δ-CNO	1.349	1.402	1.467	−3.470	1446	1053	607	
Nonlinear Saddle Points ($^2A''$)								
CNO → Δ-CNO	1.284	1.366	2.065	−2.673	1456	1033	500i	
NCO → Δ-CNO	1.293	1.844	1.424	−2.537	1399	515	713i	
Nonlinear Saddle Point ($^2A'$)								
CNO	*1.237*	*1.478*	*1.715*	*−1.201*	*1674*	*739*	*690i*	
Nonlinear Second-Order Saddle Points								
C−ON	2.639	1.184	1.819	0.128	1531	228i	435i	
	1.971	*1.232*	*1.711*	*0.533*	*1373*	*354i*	*494i*	
O−CN	1.211	2.217	2.484	−1.091	1745	247i	331i	
	1.207	*2.252*	*2.427*	*−1.136*	*1986*	*203i*	*296i*	

[a] All distances are in Å. All energies are relative to C + NO and are quoted in eV, and the harmonic frequencies are in cm^{-1}. Data for ^{2}A″ and ^{2}A′ (italic) are given.

an expression for the long-range energy. These calculations and the features of the surfaces are presented in our previous papers.[15,17] In Table 4, the energetics of the arrangement channels are presented. Good agreement between our surfaces and experiment is found, except for the exothermicity of the N(^{2}D) + CO channel which is underestimated by 0.2 eV. The most important stationary points are summarized in Table 5. The reason for the linear species not being strictly equal on the two surfaces is that the surface fitting was performed separately for each surface. The differences in bending frequencies are however natural because these depend on the potential as a function of bending angle. We have in our calculations neglected the couplings between the surfaces and treated them separately.

2.1.1. The C + NO Channel. In Figures 1 and 2, the differences between the $^2A'$ and $^2A''$ surfaces are clearly visible for the C + NO channel. For nonlinear geometries, the surfaces exhibit quite different behaviors. Whereas the $^2A'$ surface is repulsive for the perpendicular approach of carbon toward NO, there is a triangular potential minimum, Δ-CNO, on the $^2A''$ surface. Both surfaces have potential barriers for an angled

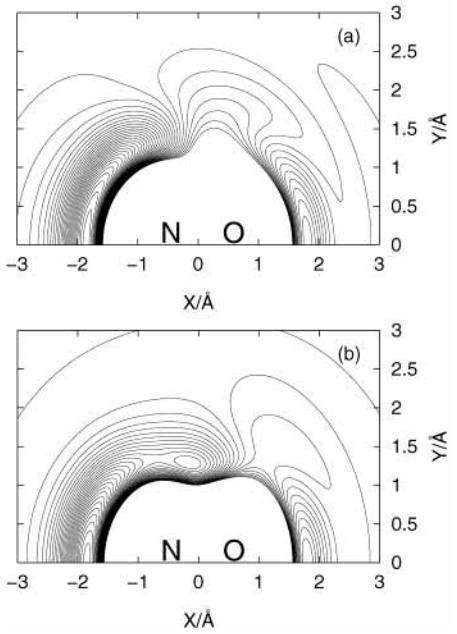

Figure 1. Polar contour plots of the C + NO channel for (a) $^2A'$ and (b) $^2A''$. NO is kept at its equilibrium distance. The potential curves range from −4.0 to 0.95 eV with a spacing of 0.15 eV. The energies are relative to the C + NO asymptotic energy.

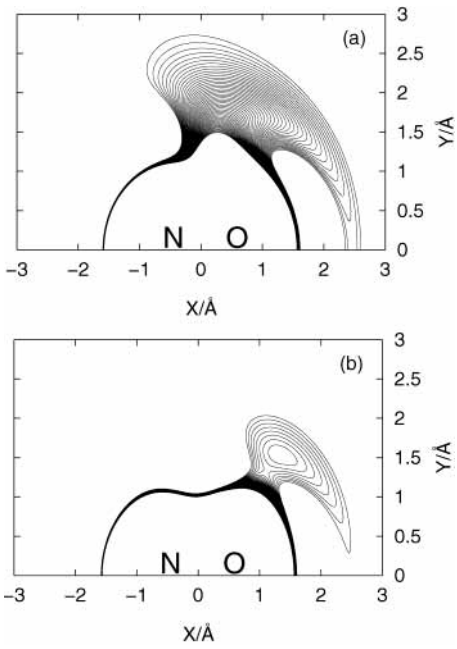

Figure 2. Polar contour plots of the C + NO channel for (a) $^2A'$ and (b) $^2A''$. NO is kept at its equilibrium distance. Only regions where the potential energy is higher than the C + NO asymptotic energy are plotted, with potential curves ranging from 0 to 1.0 eV with 0.02 eV spacings. The energies are relative to the C + NO asymptotic energy.

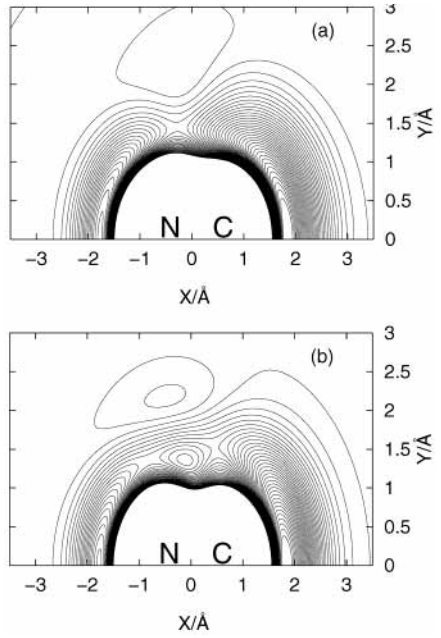

Figure 3. Polar contour plots of the O + CN channel for (a) $^2A'$ and (b) $^2A''$. CN is kept at its equilibrium distance. The potential curves range from −6.5 to 1.0 eV with a spacing of 0.15 eV. The energies are relative to the C + NO asymptotic energy.

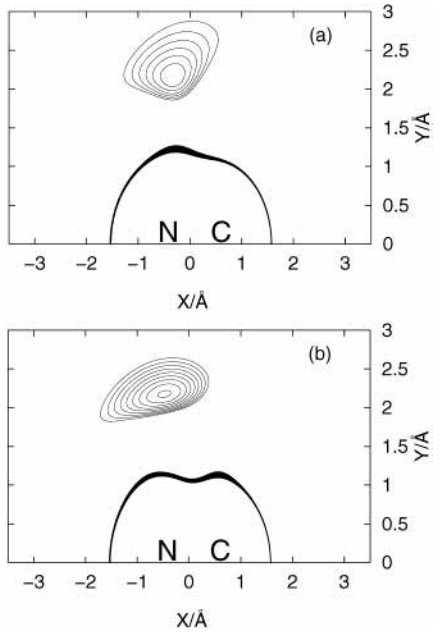

Figure 4. Polar contour plots of the O + CN channel for (a) $^2A'$ and (b) $^2A''$. CN is kept at its equilibrium distance. Only regions where the potential energy is higher than the O + CN asymptotic energy are plotted, with potential curves ranging from 0 to 1.0 eV with 0.02 eV spacings. The energies are relative to the O + CN asymptotic energy.

approach of C toward the oxygen end of NO. The barrier heights are however quite different on the two surfaces: 0.53 eV for $^2A'$ and 0.13 eV for $^2A''$.

2.1.2. The O + CN Channel. As shown in Figures 3 and 4, the $^2A'$ and $^2A''$ surfaces are quite similar for the O + CN channel compared to the situation in the C + NO channel. There are barriers for the perpendicular approach of O toward CN of similar height on both surfaces (0.09 eV on $^2A'$ and 0.14 eV on $^2A''$). However, there is the Δ-CNO minimum inbetween CNO and NCO on the $^2A''$ surface. This facilitates the rearrangement between the different minima.

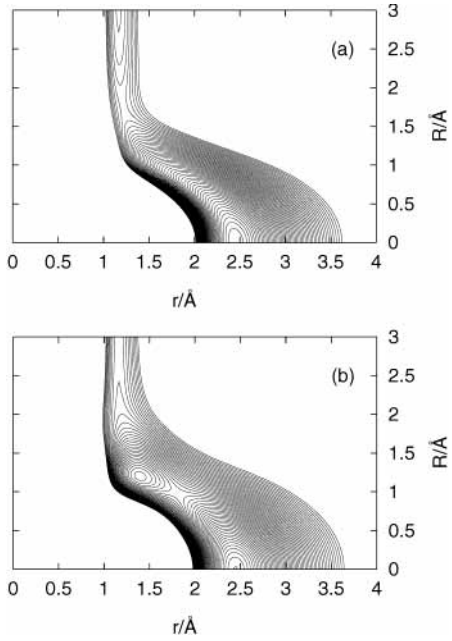

Figure 5. Contour plot of the potential energy as a function of the Jacobi coordinates r and R for the C + NO channel. The angle θ is kept fixed at 90° (perpendicular approach of C toward the NO center of mass). The potential curves range from −6.9 to +1.2 eV with a spacing of 0.15 eV. The energies are relative to the C + NO asymptotic energy. (a) $^2A'$ surface (b) $^2A''$ surface.

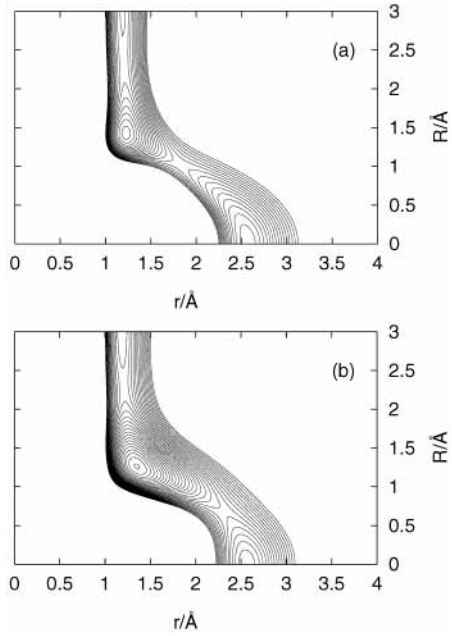

Figure 6. Contour plot of the potential energy as a function of the Jacobi coordinates r and R for the O + CN channel. The angle θ is kept fixed at 90° (perpendicular approach of O toward the CN center of mass). The potential curves range from −3.45 to +1.2 eV with a spacing of 0.15 eV. The energies are relative to the C + NO asymptotic energy. (a) $^2A'$ surface (b) $^2A''$ surface.

2.1.3. The Δ-CNO Minimum. The triangular minimum, Δ-CNO, is quite important for the reactivity on the $^2A''$ surface. In Figures 5−7, the surfaces are plotted for the perpendicular approach of the atom toward the diatom center of mass, i.e., at a Jacobi angle of 90°, for the three arrangement channels. It is seen that through the Δ-CNO minimum the system has a more accessible pathway between the different linear minima and also between reactants and products on the $^2A''$ surface compared to the $^2A'$ surface.

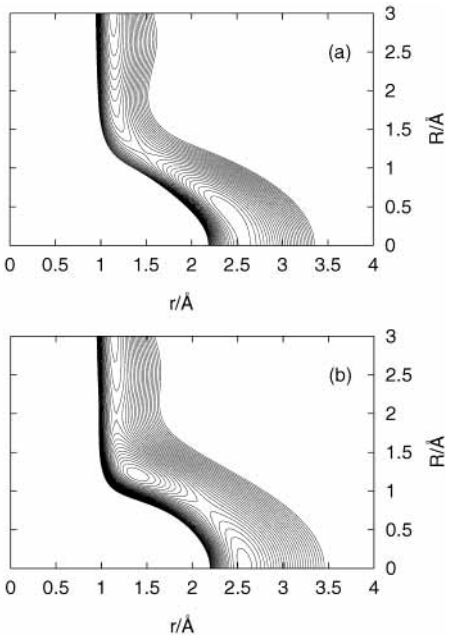

Figure 7. Contour plot of the potential energy as a function of the Jacobi coordinates r and R for the N + CO channel. The angle θ is kept fixed at 90° (perpendicular approach of N toward the CO center of mass). The potential curves range from −4.2 to +1.2 eV with a spacing of 0.15 eV. The energies are relative to the C + NO asymptotic energy. (a) $^2A'$ surface (b) $^2A''$ surface.

2.2. Quasiclassical Trajectories. We have run quasiclassical trajectories (QCT) on the two potential energy surfaces described above. The QCT are calculated by integrating Newton's equation of motion using the RADAU integrator.[18] This integrator has been shown to be both efficient and accurate for molecular dynamics applications.[19] We have performed calculations for the C + NO and O + CN reactions for different temperatures. For these calculations, thermal rate coefficients have been calculated as (for a specific product channel i):

$$k_i(T) = \left(\frac{8k_BT}{\pi\mu}\right)^{1/2} \pi b_{\max,i}{}^2 \frac{N_{r,i}}{N} \tag{4}$$

where N is the total number of trajectories, $N_{r,i}$ the number of reactive trajectories, $b_{\max,i}$ is the largest impact parameter, and μ is the reduced mass of the reactants. The sampling procedures have been described previously, see ref 15. The $k_i(T)$ are calculated separately for the $^2A'$ and $^2A''$ surfaces.

In our trajectory calculations, a collision complex is considered to have formed if at least one minimum distance exchange occurs, i.e., the shortest distance between any two nuclei does not involve the same pair of nuclei at all times.

2.3. Electronic Structure Calculations Including Spin−Orbit Coupling. For the long-range part of the O + CN channel we have performed new state average CASSCF calculations for the lowest electronic states of each symmetry. An active space with 13 electrons in 11 orbitals was used, where all 1s orbitals and the 2s orbital on oxygen were held inactive. For all calculations, we used an atomic natural orbital (ANO) basis set with the 14s9p4d3f primitive set contracted to 4s3p2d1f. Further the RASSI−SO (restricted active space state interaction with spin−orbit coupling)[20] method was employed to calculate spin−orbit matrix elements between the electronic states. For these calculations, the Douglas-Kroll Hamiltonian[21,22] was used. To form the full spin−orbit potential matrix, these off-diagonal matrix elements have been supplemented with diagonal elements, being energies of the involved states calculated at the multistate CASPT2 level employing the g_1 Fock matrix with the 1s orbitals frozen. By diagonalizing the spin−orbit matrix, we have as diagonal elements obtained the nine lowest adiabatic spin−orbit states, i.e., those that adiabatically correlate to the fine structure states of the reactants, as described in the next section. All electronic structure calculations were performed using the MOLCAS 5.2 program package.[23]

2.4. Electronic Degeneracy Factors. From the combination of the electronic states of the reactants, one obtains 36 (9 × 4) electronic states adiabatically correlating with C(^{3}P) and NO($X^2\Pi$) and 18 (9 × 2) with O(^{3}P) and CN($X^2\Sigma^+$). Because the CNO system has an odd number of electrons, the electronic states come in degenerate pairs, Kramers doublets, because of time-reversal invariance.[24,25] Thus, we have 18 *distinct* potential energy surfaces for C(^{3}P) + NO($X^2\Pi$) and 9 for O(^{3}P) + CN (($X^2\Sigma^+$). Conversely, our $^2A'$ and $^2A''$ surfaces correspond to *four* electronic states.

From adiabatic correlations between the potential energy surfaces and specific fine structure states of the reactants, we obtain what we refer to as electronic degeneracy factors. These describe the fraction of the thermal population on the reactant electronic states that may lead to reaction. This, of course, requires some a priori knowledge of which potential energy surfaces have readily available pathways to the products.

A general expression for an electronic degeneracy factor of an A + BC reaction is given by

$$f(T) = \frac{Q_{A-BC}(T)}{Q_A(T)Q_{BC}(T)} \tag{5}$$

where $Q_A(T)$ and $Q_{BC}(T)$ are reactant electronic partition functions, and $Q_{A-BC}(T)$ is the partition function of the reactant fine structure states that adiabatically correlate with the surfaces leading to reaction.

Assuming that the $^2A'$ and $^2A''$ surfaces are the only surfaces available for reaction we have multiplied the "raw" rate coefficients (eq 4) obtained from our trajectory calculations by appropriate electronic degeneracy factors. To be able to compare the results from the separate surfaces to each other and to experiment, we have as a first approach considered the case when the dynamics takes place on one surface *or* the other. Thus, the electronic degeneracy factors presented below are constructed for this situation.

For the O + CN reaction, it is assumed that two out of the five $J = 2$ states of the oxygen atom correlate with the reactive surfaces. CASPT2 calculations of the fine-structure states in the long-range part of this system, performed as detailed in section 2.3, strongly indicate that this is a proper description, see Figure 8. This gives the following expression for the electronic degeneracy factor

$$f^{O+CN}(T) = \frac{2}{5 + 3\exp(-228/T) + \exp(-326/T)} \tag{6}$$

For the C + NO reaction, the choice of electronic degeneracy factor seems to be more difficult. We were not able calculate the fine-structure states for the complex CNO as there were problems of converging to the correct states, mainly because the number of states is twice as large as for O + CN. Lacking this information, we shall here describe two approaches for choosing electronic degeneracy factors for the C + NO reaction.

In the first approach, it is assumed that the reactive surfaces ($^2A'$ and $^2A''$) correlate with C($^3P_0$) + NO($X^2\Pi_{1/2}$) and

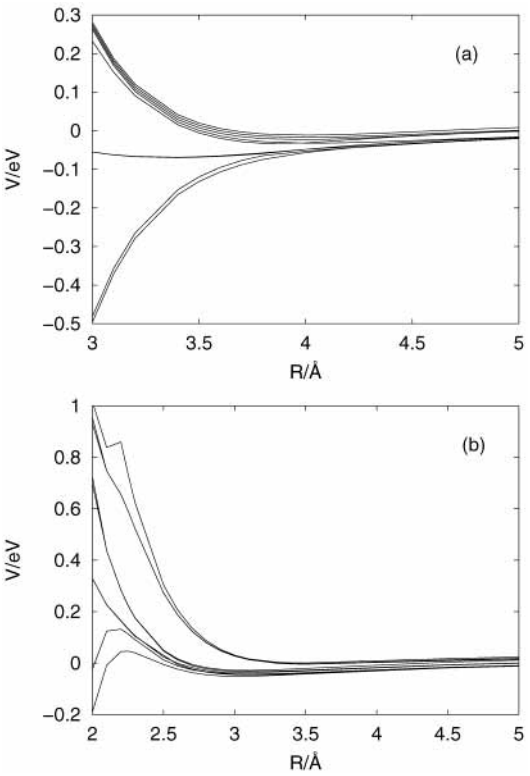

Figure 8. Profiles of the nine lowest fine-structure potential surfaces for the O + CN channel calculated at the CASSCF/CASPT2 level of accuracy. The profiles correspond to Jacobi angles (a) 0° (O−CN) and (b) 90°. Energies are relative to the $O(^3P_2)$ + $CN(X^2\Sigma^+)$ asymptotic energy.

$C(^3P_0)$ + $NO(X^2\Pi_{3/2})$. In this way, the following factor is obtained

$$f_{00}^{C+NO}(T) = \frac{1}{1 + 3\exp(-23.6/T) + 5\exp(-62.4/T)} \quad (7)$$

This is derived from the fact that the $^2\Pi$ ground states of the linear intermediates (CNO, NCO, and CON) are split into two states with $\Omega = 1/2$ and 3/2, respectively, where Ω is the quantum number of the total electronic angular momentum about the internuclear axis. Combining the $J = 0$ state of the carbon atom and the $\Omega = 1/2$ (or 3/2) states of NO will give states with $\Omega = 1/2$ (or 3/2) for the compound system. This approach is the one taken in connection with the ACCSA calculations presented in the paper by Geppert et al.[26]

We now argue against using the above electronic degeneracy factor. From the experiment, it is inferred that even though the electronic ground state of NO is $^2\Pi_{1/2}$[27], the ground states of CNO[28] and NCO[16], are both $^2\Pi_{3/2}$. Thus, surfaces of different Ω will have to cross somewhere as asymptotically the $C(^3P_1)$ + $NO(X^2\Pi_{1/2})$ and $C(^3P_2)$ + $NO(X^2\Pi_{1/2})$ states are below the $C(^3P_0)$ + $NO(X^2\Pi_{3/2})$ states. Furthermore, for nonlinear geometries (C_s symmetry) surfaces of $^2A'$ and $^2A''$ symmetries will have avoided crossings among themselves, disregarding the values of Ω (and Λ, the quantum number of orbital angular momentum about the axis) for linear geometries ($C_{\infty v}$ symmetry). In the far long-range region where the interaction potential is smaller in magnitude than the splitting of the spin−orbit states, the system is best described by Hund's coupling case (c) (*jj* coupling) as opposed to the strong interaction region where Hund's case (a) (*LS* coupling) is more appropriate.[29] This means that the A' and A'' symmetries lose their significance at long range and that *all* adiabatic surfaces have avoided crossings

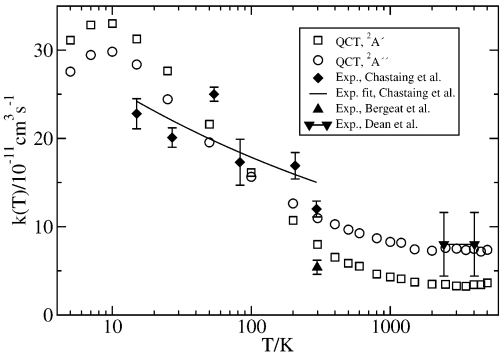

Figure 9. Total thermal rate coefficients for the C + NO reaction. Open symbols correspond to calculated rate coefficients for the $^2A'$ and $^2A''$ surfaces, and filled symbols correspond to experimental results (refs 32−34).

at nonlinear geometries, since in this case there is only one possible symmetry (half-integer spin states). If the above choice of electronic degeneracy factor is to be valid, then nonadiabatic transitions must be effective in taking the system from $C(^3P_0)$ + $NO(X^2\Pi_{3/2})$ to the lowest PES during the course of approach of the reactants.

The second approach for determining an electronic degeneracy factor is as follows. There is the possibility that apart from $C(^3P_0)$ + $NO(X^2\Pi_{1/2})$, which correspond to the states of lowest energy at infinite separation of the reactants, also $C(^3P_1)$ + $NO(X^2\Pi_{1/2})$ may correlate with the reactive surfaces, since this can give states with $\Omega = 3/2$ for the compound system and also because they are the states of second lowest energy at infinite separation. This choice would be natural if one treats the dynamics as strictly adiabatic, i.e., not allowing transitions between surfaces. In the paper by Beghin et al.,[30] it was argued that for C + NO the system would be well described within a single surface approximation for temperatures below 500 K. This analysis was based on the Massey criterion, as described by Graff and Wagner[31] in their study of the O + OH reaction. An adiabatic picture, as described above, gives an electronic degeneracy factor of the form

$$f_{01}^{C+NO}(T) = \frac{2 + 2\exp(-23.6/T)}{[1 + 3\exp(-23.6/T) + 5\exp(-62.4/T)][2 + 2\exp(-172.4/T)]} \quad (8)$$

The temperature regime where the adiabatic approximation is assumed to be valid is also where the electronic degeneracy factors have the largest effect on the calculated rate coefficients. The use of $f_{01}^{C+NO}(T)$ gives at most about 60% larger $k(T)$ than $f_{00}^{C+NO}(T)$ (at 50 K), whereas the difference at high temperatures ($T \geq 1500$ K) is less than 5%. We have chosen to use $f_{01}^{C+NO}(T)$ in the present work.

3. Results and Discussion

We have performed quasiclassical trajectory calculations for 23 temperatures in the range 5−5000 K for the C + NO and O + CN reactions on both the $^2A'$ and $^2A''$ surfaces. For each reaction, surface, and temperature, 16 000 trajectories have been run. The total rate coefficients are presented in Figures 9 and 10. The branching fractions for the C + NO reaction, defined as $k_2/(k_1 + k_2)$, are shown in Figure 11.

For the C + NO reaction, it is seen that both surfaces give good agreement with experiment at temperatures at and below 300 K.[32] Comparing the branching fractions it is seen that it is

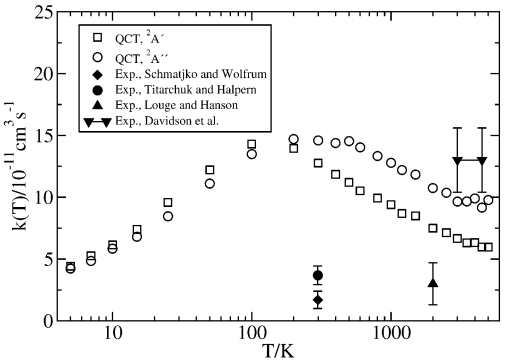

Figure 10. Total thermal rate coefficients for the O + CN reaction. Open symbols correspond to calculated rate coefficients for the $^2A'$ and $^2A''$ surfaces, and filled symbols correspond to experimental results (refs 35−38).

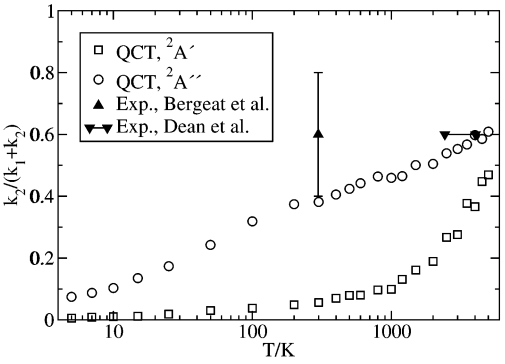

Figure 11. Branching fractions for the C + NO reaction. k_1 is the rate coefficient for O + CN formation and k_2 the rate coefficient for N + CO formation. Open symbols correspond to calculated branching fractions for the $^2A'$ and $^2A''$ surfaces and filled symbols correspond to experimental results (refs 33 and 34).

only the $^2A''$ which is close to the measured value of Bergeat et al.[33] Also comparing to the high-temperature data of Dean et al.,[34] the $^2A''$ surface gives results in very good agreement with these, both for rate coefficients and branching fractions. On the $^2A'$ the production of N + CO is quite low for almost the whole temperature range. It is only at very high temperatures that this product channel becomes significant.

Whereas the calculated C + NO rate coefficients show a peak at about 10 K, the O + CN rate of reaction peaks around room temperature. This is *not* in agreement with experiment, however. The two most recent measured rate coefficients[35,36] are considerably below our calculated values, and our values are about a factor of 4 larger than the larger of these two. There are no experimental data for temperatures below 300 K. Both our surfaces show also for this reaction quite similar behavior for low temperatures, but it is only the $^2A''$ surface that compares well to the high-temperature experiments of Davidson et al.[37] The rate coefficient measured at 2000 K by Louge and Hanson,[38] contrary to the results of Davidson et al.,[37] is much lower than our results.

The differences and similarities in reactivity of the two surfaces can be understood by considering the behavior of the interaction potential. This will be discussed in the following two sections.

3.1. Reactivity of C + NO. For low temperatures, say $T \leq$ 25 K, the trajectories are guided according to the most attractive pathway, i.e., towards a (near-)linear CNO configuration, see Figure 12, which yields almost exclusively O + CN as products. For N + CO to be formed, either a nonlinear approach of C toward NO is needed to make it possible to rearrange to Δ-CNO

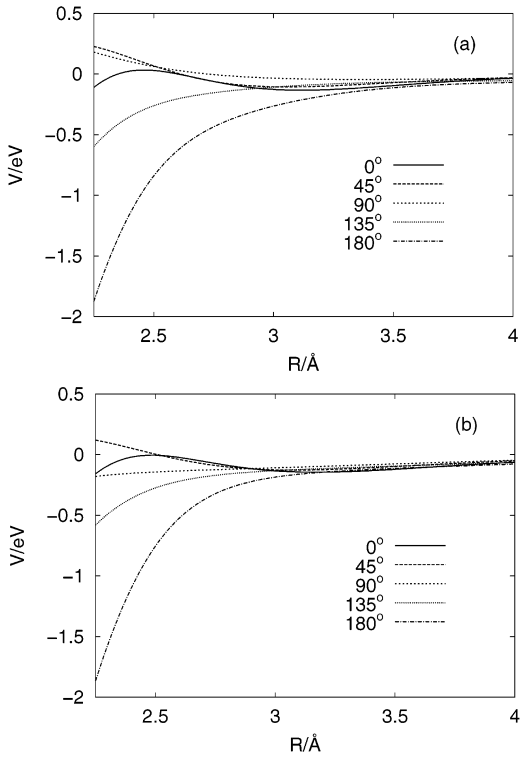

Figure 12. Profiles of the potential energy in the C + NO channel at different Jacobi angles (0°, C−ON and 180°, C−NO) for (a) the $^2A'$ and (b) the $^2A''$ surfaces. Energies are relative to the C + NO asymptotic energy.

and/or NCO or a linear approach toward the CON configuration. For these latter cases, the potential is less attactive and there is also a barrier for some angles of approach as was discussed in section 2.1.1. For $T \leq$ 200 K, the total rate coefficients do not deviate much between $^2A'$ and $^2A''$ due to the fact that for the low collision energies involved it is the long-range potential that is decisive for the reactivity. The long-range parts are in fact quite similar, which they should be as they converge asymptotically. In these cases, as was discussed above, most of the trajectories go through CNO, but on the $^2A''$ surface, the system can also proceed to Δ-CNO without barriers. This accounts for the significantly higher production of N + CO on the $^2A''$ surface compared to the $^2A'$.

As can be seen from Figure 9, with increasing temperature, the reactivities on the two surfaces start to deviate considerably, with the $^2A''$ surface being a factor of 2 or so more reactive than the $^2A'$ surface at high temperatures. This is due to the fact that Δ-CNO and thus also NCO become more readily available. This increases the number of possible reaction pathways available to the system, especially those leading to N + CO. To conclude, one can say that at low temperatures the C + NO reaction is dominated by the collinear reaction through the CNO minimum, but at higher temperatures, nonlinear reaction pathways become more important, especially on the $^2A''$ surface.

3.2. Reactivity of O + CN. As discussed in section 2.1.2, for the nonlinear approach of O toward CN, there are potential barriers on both surfaces. This makes the rate of reaction decrease with decreasing temperature below 200 K. As shown in Figure 13, the low-energy trajectories should be "drawn" into the NCO minimum as the potential is highly attractive for approach toward this minimum. Just as for the C + NO reaction, the difference in reactivity of the two surfaces at higher temperatures is due to the Δ-CNO minimum becoming more

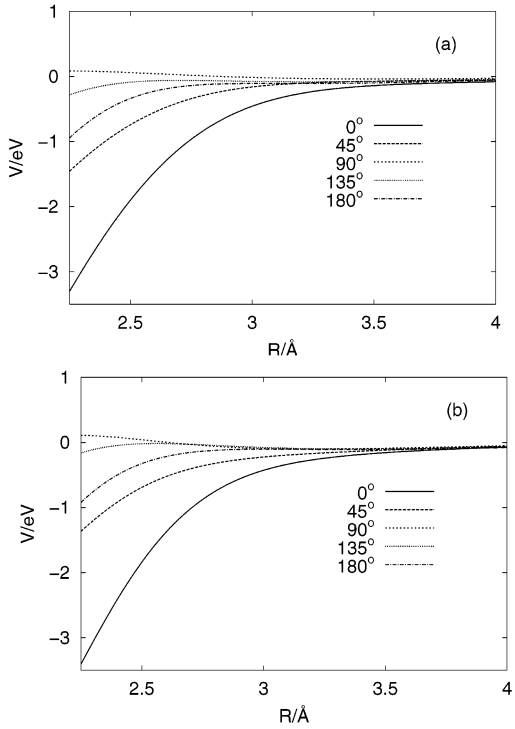

Figure 13. Profiles of the potential energy in the O + CN channel at different Jacobi angles (0°, O−CN and 180°, O−NC) for (a) the $^2A'$ and (b) the $^2A''$ surfaces. Energies are relative to the O + CN asymptotic energy.

easily available on the $^2A''$ surface. It must also be remembered that it is almost exclusively N + CO that is formed due to the C + NO channel being endothermic by about 1.2 eV. This means that trajectories entering (near-)collinearly into the CNO minimum emerge as nonreactive in most cases.

Regarding the deviation from experimental rate coefficients for this reaction, the quality of our surfaces in this channel could play a role. At long-range, the surfaces seem to be slightly too attractive; that is, the gradient of the interaction potential is too large with respect to *R*. In Figure 14, we compare new CASPT2 calculations of the two lowest fine-structure states, as described in detail in section 2.3, alongside the $^2A'$ and $^2A''$ surfaces for medium long-range distances at three angles of approach. It is seen that our surfaces seem to be somewhat too attractive. We note that the surfaces were fitted with an emphasis on the long-range part of the C + NO channel. There was also a lack of some ab initio points in the O + CN channel due to numerical problems (see ref 15). It can thus be expected that the quality of our surfaces in this latter channel is lower than for C + NO. We expect that the rate coefficients for the O + CN presented in this paper are too high in the low-temperature regime.

3.3. Rate Coefficients. Looking at experimental data it is of course impossible to discuss reactivity depending on one surface or the other. We can from experiment only extract information about what reactant states enter the reaction and what product states emerge at the other end. To compare our results to experiment, we must combine our calculated *single-surface* data into unique rate coefficients for the reactions. A simple way to do this is to just add the separate rate coefficients together, weighted with appropriate thermal factors. This however relies on the two surfaces being uncoupled whereby the dynamics occur on *either* $^2A'$ or $^2A''$. Because the CNO system exhibits the Renner−Teller effect,[16] a more complicated situation arises. Working with Born−Oppenheimer basis states, the $^2A'$ and $^2A''$ surfaces in our case would mean that for excited bending

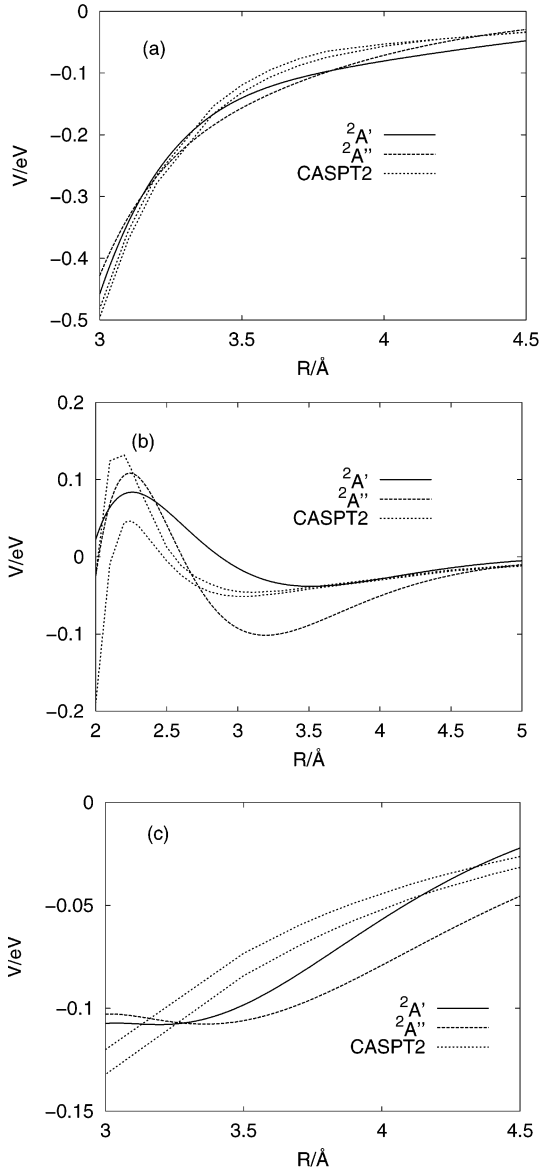

Figure 14. Profiles of the potential energy in the O + CN channel at Jacobi angles (a) 0° (O−CN), (b) 90°, and (c) 180° (O−NC). Our $^2A'$ and $^2A''$ surfaces are compared to newly performed CASPT2 calculations on the two lowest fine-structure states.

vibrational modes of the linear molecules (NCO, CNO, and CON) transitions between these states will occur.

During the course of the reaction, it is not unlikely that the system will find itself in a bending motion of a linear intermediate. Should it initially be on the $^2A'$ surface, a transition could take place that would take the system into the Δ-CNO minimum on the $^2A''$ surface. From this minimum, there is a direct pathway to the N + CO products, as we discussed in ref 17. The opposite situation, a transition from $^2A''$ to $^2A'$, would not open up any alternative pathways to the product channels.

Thus, we consider it quite possible that there is an additional "escape route" out of the interaction region on the $^2A'$ surface through the Δ-CNO minimum on the $^2A''$ surface; that is, there would be a net flux of population from $^2A'$ to $^2A''$. We thus suspect that the reactivity for trajectories initially on the $^2A'$ surface would be increased should a proper treatment of the Renner−Teller effect be included. A rigorous treatment of this effect is not trivial. Trajectory surface hopping calculations could be a way to get more insight into this interesting aspect of the dynamics.

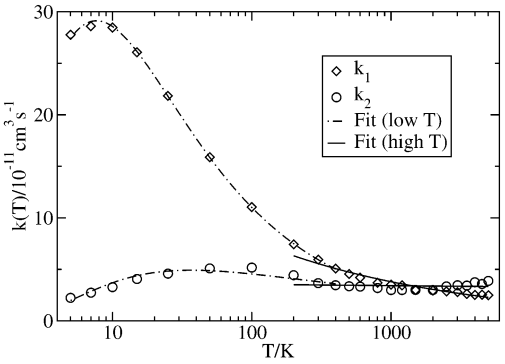

Figure 15. Recommended rate coefficients for the C + NO reaction from our calculations using eq 9 together with plotted Arrhenius type fits for two temperature regimes: 5−400 K and 200−5000 K. The rate coefficients correspond to O + CN (k_1) and N + CO (k_2) formation.

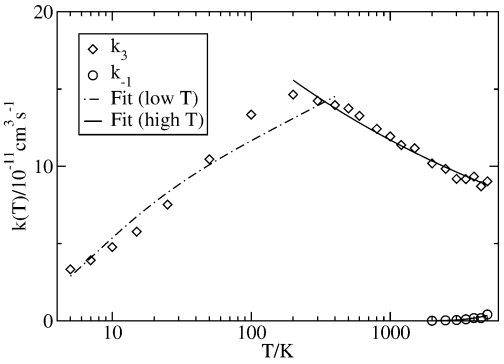

Figure 16. Recommended rate coefficients for the O + CN reaction from our calculations using eq 9 together with plotted Arrhenius type fits for two temperature regimes: 5−400 K and 200−5000 K. The rate coefficients correspond to N + CO (k_3) and C + NO (k_{-1}) formation.

Here we have chosen a simplistic approach to deal with these matters. We make the assumption that *all* complex-forming trajectories on the $^2A'$ surface make the transition to the $^2A''$ surface and proceed to the product channels on that surface. The resulting rate coefficients from this approach can be described as

$$k_i(T) = \frac{k'_c(T) + k''_c(T)}{2k'_c(T)} k''_i(T) \qquad (9)$$

where $k_i(T)$ is the rate coefficient for product channel i at temperature T, $k'_c(T)$ and $k''_c(T)$ are the rate coefficients for *complex formation*, i.e., involving both reactive and nonreactive collisions, on the $^2A'$ and $^2A''$ surfaces, respectively, and $k''_i(T)$ is the rate coefficient for product channel i on the $^2A''$ surface alone.

For near-collinear processes, it is not likely that these transitions will occur due to the fact that it is only for excited bending vibrations the Renner−Teller interaction is effective. The dynamics should in these cases be dependent on the two surfaces *separately*. As discussed above, it is only at low temperatures that the reactions are collinearly dominated. At these temperatures, the total rate coefficients on the two surfaces are however quite similar, meaning that there would be no great effect on the "composite" rate coefficients. It could however be significant for the branching fraction of the C + NO reaction, because N + CO production is so much lower on the $^2A'$ surface than on $^2A''$ at low temperatures.

Using eq 9, we have calculated rate coefficients which are the recommended results to compare to experiment, according to our discussion above. These rate coefficients differ from the ones calculated using the $^2A''$ surface, by factors lying between 0.8 and 1.1. The results are presented in Figures 15 and 16 together with fits to an Arrhenius type expression of the form

$$k(T) = A(T/298)^{\beta} e^{-\gamma/T} \qquad (10)$$

The fits have been performed for a low-temperature (5−400 K) and a high-temperature (200−5000 K) regime separately, and the parameters are given in Table 6.

4. Conclusions

Our results support the experimental rate coefficients of Chastaing et al.[32] and Dean et al.[34] for the C + NO reaction and Davidson et al.[37] for the O + CN reaction at high temperatures. However, for the O + CN reaction at room temperature, our results disagree quite strongly with the available experimental data. As was discussed in the text, we believe that we overestimate these rate coefficients for low temperatures, but we cannot predict by how much. Because the detailed knowledge of the rate coefficients for this reaction in the low-temperature regime is of utmost importance for astrochemical applications, it is our hope that low-temperature experiments will be performed for this important reaction.

TABLE 6: Parameters for Arrhenius Type Expressions Based on eqs 9 and 10

	$A/10^{-11}$ cm^3 s^{-1}	β	γ/K
$T = 5-400$ K			
k_1, C + NO → O + CN	6.055	−0.59	4.51
k_2, C + NO → N + CO	3.907	−0.21	7.68
k_3, O + CN → N + CO	14.164	0.13	5.30
$T = 200-5000$ K			
k_1, C + NO → O + CN	5.572	−0.315	0
k_2, C + NO → N + CO	3.488	−0.0153	0
k_3, O + CN → N + CO	14.512	−0.178	0
k_{-1}, O + CN → C + NO	5.369	0	13 750

The QCT calculations presented in this paper are mostly in good agreement with experiment. There are several ways of investigating the accuracy of our calculations, all of them, however, quite computationally demanding:

(i) For the lower temperatures considered in this work, there could be pronounced quantum effects on the nuclear dynamics. Quantum dynamics calculations for C + NO have been performed by Monnerville et al.[39] and Abrol et al.[40] in 2D and by Monnerville et al.[41] in 3D on a simpler PES with only the CNO minimum included. Collinear (2D) calculations are quite feasible, but full 3D calculations on the present surfaces would be quite heavy and time-consuming due to the presence of several deep potential wells.

(ii) At the higher temperatures considered in this work, more than just the two lowest potential energy surfaces may become accessible as alternative reaction pathways. Preliminary CASPT2 calculations suggest that for instance a $^4A''$ state which correlates with all electronic ground states of the arrangement channels could become important. This is the only *adiabatic* pathway from C + NO and O + CN to N(^{4}S) + CO($X^1\Sigma^+$).

(iii) It is highly probable that non-Born−Oppenheimer effects play a role in the dynamics of this system. This does not only involve the Renner−Teller effect as discussed in this paper but also spin−orbit and derivative couplings between the adiabatic potential energy surfaces. There are crossings of the $^4A''$ surface discussed in the previous paragraph and the $^2A'$ and $^2A''$ surfaces used in our calculations (see ref 42). Because there are nonzero

spin−orbit matrix elements between these states this could be an important *nonadiabatic* pathway to $N(^4S) + CO(X^1\Sigma^+)$.

Acknowledgment. This work has been supported by the Swedish Research Council (Vetenskapsrådet). Dr. Roland Lindh and Prof. Björn Roos, Lund University, are gratefully acknowledged for support and discussions regarding the MOLCAS calculations.

References and Notes

(1) Herbst, E.; Klemperer, W. *Astrophys. J.* **1973**, *185*, 505.
(2) Pineau des Forêts, G.; Roueff, E.; Flower, D. R. *Mon. Not. R. Astron. Soc.* **1990**, *244*, 668.
(3) Herbst, E.; Lee, H.-H.; Howe, D. A.; Millar, T. J. *Mon. Not. R. Astron. Soc.* **1994**, *268*, 335.
(4) Federman, S. R.; Strom, C. J.; Lambert, D. L.; Cardelli, J. A.; Smith, V. V.; Joseph, C. L. *Astrophys. J.* **1994**, *424*, 772.
(5) Gerin, M.; Viala, Y.; Pauzat, F.; Ellinger, Y. *Astron. Astrophys.* **1992**, *266*, 463.
(6) Glarborg, P.; Miller, J. A.; Kee, R. J. *Combust. Flame* **1986**, *65*, 177.
(7) Thorne, L. R.; Branch, M. C.; Chandler, D. W.; Kee, R. J.; Miller, J. A. *21st Symposium (International) on Combustion*; The Combustion Institute: Pittsburgh, PA, 1986; p 965.
(8) Miller, J. A.; Bowman, C. T. *Prog. Energy Combust. Sci.* **1989**, *15*, 287.
(9) Glarborg, P.; Alzueta, M. U.; Dam-Johansen, K.; Miller, J. A. *Combust. Flame* **1998**, *115*, 1.
(10) Lindstedt, R. P.; Lockwood, F. C.; Selim, M. A. *Combust. Sci. Technol.* **1995**, *108*, 231.
(11) Juchmann, W.; Latzel, H.; Shin, D. I.; Peiter, G.; Dreier, T.; Volpp, H.-R.; Wolfrum, J.; Lindstedt, R. P.; Leung, K. M. *27th Symposium (International) on Combustion*; The Combustion Institute: Pittsburgh, PA, 1998; p 469.
(12) Sick, V.; Hildenbrand, P.; Lindstedt, P. *27th Symposium (International) on Combustion*; The Combustion Institute: Pittsburgh, PA, 1998; p 1401.
(13) Schulz, C.; Volpp, H.-R.; Wolfrum, J. In *Chemical Dynamics in Extreme Environments*; Dressler, R. A., Ed.; World Scientific: Singapore, 2001; p 206.
(14) Smoot, L. D.; Hill, S. C.; Xu, H. *Prog. Energy Combust. Sci.* **1998**, *24*, 385.
(15) Andersson, S.; Marković, N.; Nyman, G. *Phys. Chem. Chem. Phys.* **2000**, *2*, 613.
(16) Herzberg, G. *Molecular Spectra and Molecular Structure. III. Electronic Spectra of Polyatomic Molecules*; Van Nostrand: Princeton, NJ, 1966.
(17) Andersson, S.; Marković, N.; Nyman, G. *Chem. Phys.* **2000**, *259*, 99.
(18) Everhart, E. In *Dynamics of Comets: Their Origin and Evolution*; Carusi, A., Valsecchi, G. B., Eds.; Reidel: Dordrecht, The Netherlands, 1985; p 185.
(19) Bolton, K.; Nordholm. S. *J. Comput. Phys.* **1994**, *113*, 320.
(20) Malmqvist, P.-Å.; Roos, B. O.; Schimmelpfennig, B. *Chem. Phys. Lett.* **2002**, *357*, 230.
(21) Douglas, N.; Kroll, N. M. *Ann. Phys.* **1974**, *82*, 89.
(22) Hess, B. *Phys. Rev. A* **1986**, *33*, 3742.
(23) Andersson, K.; Barysz, A.; Bernhardsson, A.; Blomberg, M. R. A.; Carissan, D.; Cooper, L.; Cossi, M.; Fleig, T.; Fülscher, M. P.; Gagliardi, L.; de Graaf, C.; Hess, B. A.; Karlström, G.; Lindh, R.; Malmqvist, P.-Å.; Neogrády, P.; Olsen, J.; Roos, B. O.; Schimmelpfennig, B.; Schütz, M.; Seijo, L.; Serrano-Andrés, L.; Siegbahn, P. E. M.; Stålring, J.; Thorsteinsson, T.; Veryazov, V.; Wierzbowska, M.; Widmark, P.-O. *MOLCAS version 5.2*; Lund University: Sweden, 2001.
(24) Tinkham, M. *Group Theory and Quantum Mechanics*; McGraw-Hill: New York, 1964.
(25) Yarkony, D. *J. Phys. Chem.* **1996**, *100*, 17439.
(26) Geppert, W. D.; Reignier, D.; Stoecklin, T.; Naulin, C.; Costes, M.; Chastaing, D.; Le Picard, S. D.; Sims, I. R.; Smith, I. W. M. *Phys. Chem. Chem. Phys.* **2000**, *2*, 2873.
(27) Huber, K. P.; Herzberg, G. *Molecular Spectra and Molecular Structure. IV. Constants of Diatomic Molecules*; Van Nostrand: New York, 1979.
(28) Ramsay, D. A.; Winnewisser, M. *Chem. Phys. Lett.* **1983**, *96*, 502.
(29) Zare, R. N. *Angular Momentum*; Wiley: New York, 1988.
(30) Beghin, A.; Stoecklin, T.; Rayez, J. C. *Chem. Phys.* **1995**, *195*, 259.
(31) Graff, M. M.; Wagner, A. F. *J. Chem. Phys.* **1990**, *92*, 2423.
(32) Chastaing, D.; Le Picard, S. D.; Sims, I. R. *J. Chem. Phys.* **2000**, *112*, 8466.
(33) Bergeat, A.; Calvo, T.; Dorthe, G.; Loison, J. C. *Chem. Phys. Lett.* **1999**, *308*, 7.
(34) Dean, A. J.; Hanson, R. K.; Bowman, C. T. *J. Phys. Chem.* **1991**, *95*, 3180.
(35) Schmatjko, K. J.; Wolfrum, J. *Ber. Bunsen-Ges. Phys. Chem.* **1978**, *82*, 419.
(36) Titarchuk, T. A.; Halpern, J. B. *Chem. Phys. Lett.* **1995**, *232*, 192.
(37) Davidson, D. F.; Dean, A. J.; DiRosa, M. D.; Hanson, R. K. *Int. J. Chem. Kinet.* **1991**, *23*, 1035.
(38) Louge, M. Y.; Hanson, R. K. *Int. J. Chem. Kinet.* **1984**, *16*, 231.
(39) Monnerville, M.; Halvick, P.; Rayez, J. C. *J. Chem. Soc., Faraday Trans.* **1993**, *89*, 1597.
(40) Abrol, A.; Wiesenfeld, L.; Lambert, B.; Kuppermann, A. *J. Chem. Phys.* **2001**, *114*, 7461.
(41) Monnerville, M.; Péoux, G.; Briquez, S.; Halvick, P. *Chem. Phys. Lett.* **2000**, *322*, 157.
(42) Minaev, B. F.; Ivanova, N. M.; Muldahmetov, Z. M. *Spectrosc. Lett.* **1989**, *22*, 901.
(43) Lindackers, D.; Burmeister, M.; Roth, P. *23rd Symposium (International) on Combustion*; The Combustion Institute: Pittsburgh, Pa, 1990; p 251.
(44) Braun, W.; Bass, A. M.; Davis, D. D.; Simmons, J. D. *Proc. R. Soc. A* **1969**, *312*, 417.
(45) Husain, D.; Kirsch, L. J. *Chem. Phys. Lett.* **1971**, *8*, 543.
(46) Husain, D.; Young, A. N. *J. Chem. Soc., Faraday Trans. 2* **1975**, *71*, 525.
(47) Becker, K. H.; Brockmann, K. J.; Wiesen, P. *J. Chem. Soc., Faraday Trans. 2* **1988**, *84*, 455.
(48) Dorthe, G.; Caubet, Ph.; Vias, Th.; Barrère, B.; Marchais, J. *J. Phys. Chem.* **1991**, *95*, 5109.
(49) Boden, J. C.; Thrush, B. A. *Proc. R. Soc. London A* **1968**, *305*, 107.
(50) Moore, C. E. *United States Department of Comm., NBS* 1971, *1*.